京都大学防災研究所年報　第51号B　平成20年6月
Annuals of Disas. Prev. Res. Inst., Kyoto Univ., No. 51 B, 2008

Effects of Groins on the Flow and Bed Deformation in Non-Submerged Conditions

Hiroshi TERAGUCHI*, Hajime NAKAGAWA, Yasunori MUTO,
Yasuyuki BABA and Hao ZHANG

*Graduate School of Engineering, Kyoto University

Synopsis

This paper presents the results obtained from the studies on turbulent flow and bed deformation around groins with experimental and numerical methods. Two impermeable or permeable groins were positioned on the left side of the model channel. The velocity distributions around the groins were measured under non-submerged conditions. In the case with impermeable groins, the local scour hole around the upstream groin resulted deeper than that of the case with permeable ones. A 3D numerical model based on unstructured meshes was developed. The numerical results for velocity distributions have been compared with those of the experimental measurements and show good agreement.

Keywords: groins, non-submerged, 3D numerical model, unstructured meshes

1. Introduction

The groin is one of the structures that is constructed in natural rivers or streams to either protect the banks from erosion or maintain navigation safety (Uijttewaal, 2005). Nowadays, groins are also constructed in rivers for the preservation and maintenance of ecosystems because diversified flow around groins creates conditions suitable for riverbank vegetation and aquatic biota (Carling et al., 1996; Schwartz and Kozerski, 2003).

Considering permeability of the structure, groins are classified into two types: impermeable ones and permeable ones. The first type is generally constructed using local rocks, gravels or gabions and the second one consists of rows of piles, bamboo or timbers (Klaasen et al, 2002). The two types of groins affect the flow field and sediment transport in different ways and result in various flow patterns and bed morphologies (Zhang, 2005; Zhang et al., 2006a). However, the morphological impacts of groins are not completely understood. Normally, the deepening of the main channel is a desirable result, but local scour around the groin toes and deposition in the main channel are unwanted with respect to the stability of the groin structure and the availability of channel width for the purpose of navigation (Garde et al., 1961; Gill, 1972). For a better understanding of the flow and/or bed deformation in groin fields, many studies have been conducted in case of single groin (Kuhnle, 2002). But in practice, groins are usually organized in a group, so a lot of studies are still needed.

This study intends to investigate the flow and bed deformation around two impermeable or permeable groins. Both laboratory experiments and numerical simulations are conducted. Experiments are able to provide reliable information under specific and controlled conditions. The similarities in process like flow separation will allow more generic applications for validate modeling tools. In view of these, a 3D numerical model based on unstructured meshes was developed.

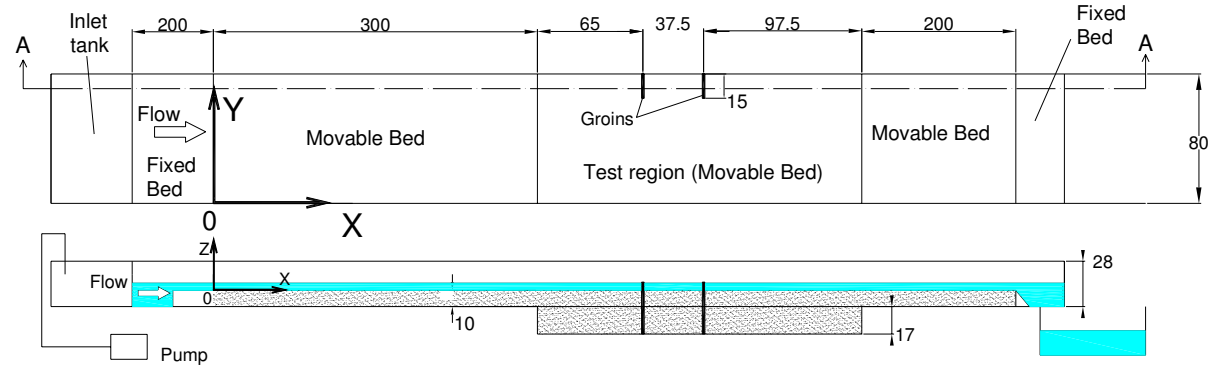

unit: cm

Fig. 1 Experimental set-up (top view, top; longitudinal view (section A-A),bottom,not to scale)

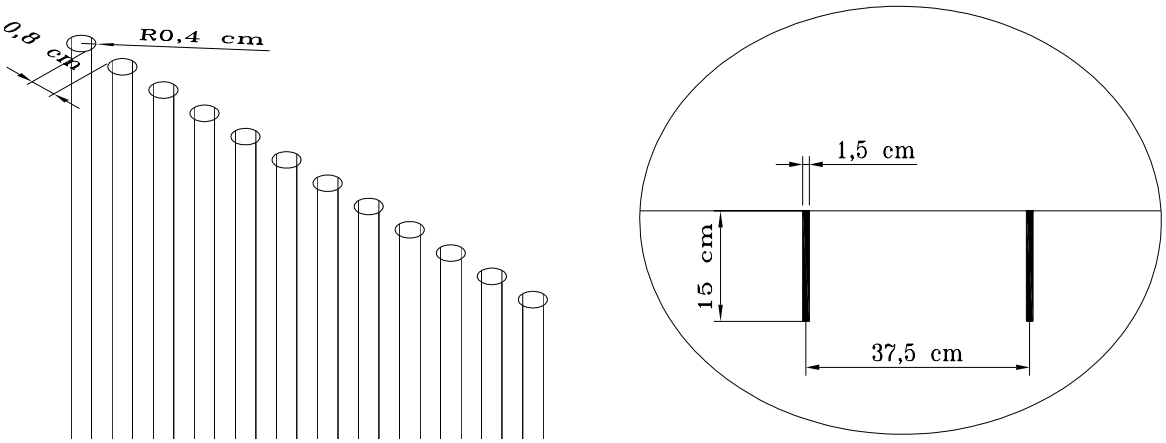

Fig. 2 Details of permeable groin (left side) and groins position and geometry (right side).

2. Laboratory Experiment

The experiments were conducted at the Ujigawa Open Laboratory, DPRI, Kyoto University, in a straight flume of 10m-long, 0.80m-wide and 0.28m-deep (0.45m-deep in test region). For the present experiments, the channel bottom was adjusted to be 1/800. The detailed sketch of the experimental set-up is shown in **Fig.1**. The x-axis starts from the beginning of the movable bed, the y-axis from the right wall of the flume and the z-axis from the initial flat bed level. There is a fixed bed, made of wooden plank elevated 10cm above the bottom at the upstream entrance. The function of the wooden plank is to smoothen the flow. Two groins are placed perpendicular to the channel banks on the left side of the flume in the test region (Fig. 2). In Case 1, impermeable groins, made of wooden cuboids, are used. In Case 2, permeable groins, a series of round sticks, are designed to have a permeability of 50%.

The sediment utilized is coal with a mean diameter of 0.83mm and a specific gravity of 1.41. The experiments are conducted under uniform flow conditions. The hydraulic parameters adopted for both cases (Cases 1 and 2) are given in **Table 1**. Uniform flow condition is established by adjusting the tailgate height of the flume. Constant rate of sediment is supplied continuously from the upstream boundary of the flume to maintain the dynamic equilibrium state.

The dry sediment is mixed with water before it is supplied in order to avoid the dispersion effects. The sediment transport rate is evaluated with the bed load transport formula proposed by Ashida-Michiue (1972), but the amount of sediment is finally adjusted from some trial experiments. Five hours duration for each experiment are found sufficient for the attainment of dynamic equilibrium condition.

At the downstream boundary, a tailgate is used to control the water level. The water level is measured

with a point gauge and the bed deformation is obtained through a laser sensor after the flume has been completely drained out.

For the measurement of velocity field, cements are used to fix the final bed deformation. After fixing the bed, the same discharge is imposed to measure the flow velocities around the groins and two electromagnetic velocimeters are utilized, one with an I-shape sensor and another with an L-shape sensor. Considering the bed roughness effects there is no difference between cements and sediments (coal) that could cause changes in the velocity results.

Table 1 Details of the experimental conditions

Cases	1	2
Submergence	non-submerged	
Discharge Q(l/s)	6.50	
Mean velocity u(cm/s)	20.31	
Flow depth h(cm)	4.00	
Shear velocity u_*(cm/s)	2.22	
Shear velocity ratio u_*/u_{*c}	1.91	
Reynolds number, Re	8,132	
Froude number, Fr	0.324	

3. Numerical Model

For the time being, the numerical model is used to simulate the flow field based on fixed-bed conditions. The governing equations of proposed numerical model are based on the steady 3D RANS (Reynolds-averaged Navier-Stokes equations) and the continuity equation, which can be expressed in a Cartesian coordinate system with the tensor notation as follows.

$$u_j \frac{\partial u_i}{\partial u_j} = F_i - \frac{1}{\rho}\frac{\partial p}{\partial x_i} + \nu \frac{\partial^2 u_i}{\partial x_j \partial x_j} + \frac{1}{\rho}\frac{\partial \tau_{ij}}{\partial x_i} \quad (1)$$

$$\frac{\partial u_i}{\partial x_i} = 0 \quad (2)$$

where u_i= time-averaged velocity; x_i= Cartesian coordinate component; ρ= density of the fluid; F_i=body force; p= time-averaged pressure; ν=molecular kinematic viscosity of the fluid; $\tau_{ij} = -\rho\overline{u_i' u_j'}$, are the Reynolds stress tensors, and u_i' is the fluctuating velocity component.

The standard k-ε model is used for the turbulence closure. The Reynolds tensors are acquired through the linear constitutive equation.

$$-\overline{u_i' u_j'} = 2\nu_t S_{ij} - \frac{2}{3}k\delta_{ij} \quad (3)$$

where k= turbulence kinetic energy; δ_{ij}= the Kronecker delta; ν_t = eddy viscosity and S_{ij}= the strain-rate tensor, the latter three are expressed by

$$\delta_{ij} = \begin{cases} 1 & if \quad i = j \\ 0 & if \quad i \neq j \end{cases} \quad (4)$$

$$\nu_t = C_\mu \frac{k^2}{\varepsilon} \quad (5)$$

$$S_{ij} = \frac{1}{2}\left(\frac{\partial u_i}{\partial x_j} + \frac{\partial u_j}{\partial x_i} \right) \quad (6)$$

in which C_μ is a coefficient, and is set to be a constant and equal to 0.09, ε is the dissipation rate of the turbulence kinetic energy k.

Two transport equations as described below are employed to estimate k and ε, respectively.

$$u_j \frac{\partial \kappa}{\partial x_j} = \frac{\partial}{\partial x_j}\left(\nu + \frac{\nu_t}{\sigma_\kappa}\frac{\partial \kappa}{\partial x_j} \right) + G - \varepsilon \quad (7)$$

$$u_j \frac{\partial \varepsilon}{\partial x_j} = \frac{\partial}{\partial x_j}\left(\nu + \frac{\nu_t}{\sigma_\varepsilon}\frac{\partial \varepsilon}{\partial x_j} \right) + \left(c_{\varepsilon 1} G - c_{\varepsilon 2} \right)\frac{\varepsilon}{\kappa} \quad (8)$$

where G= the rate-of-production of the turbulence kinetic energy k, is defined as

$$G = -\overline{u_i' u_j'}\frac{\partial u_i}{\partial x_j} \quad (9)$$

and the model constants are used as suggested by Rodi (1980).

A detailed presentation about the numerical schemes, discretization methods, solution methods, equation solvers and the convergence criteria is given by Zhang et al. (2006b).

In the simulation, the inlet boundary is considered as a Dirichlet boundary and all the quantities are prescribed. The outlet boundary has been set far from the groin area, a Neumann boundary with zero gradients is assumed there. The wall function approach is adopted near impermeable boundaries. The permeable groin is expressed as a cluster of impermeable groins and each permeable groin is expressed with some fine meshes in the simulation.

The simulation sequence follows the SIMPLE

(Semi-implicit method for pressure-linked equations) procedure. At first, the momentum equations are solved for each velocity components, in which the pressure, the eddy viscosity, the turbulent kinetic energy and its dissipation rate are considered as known. The resultant velocity field is used to calculate the mass fluxes through faces of Control Volumes. After the pressure correction equation is solved, the velocity field is improved. Finally, the transport equations for the turbulent kinetic energy and its dissipation rate are solved and the eddy viscosity is updated.

The above procedures are repeated until the residual level becomes sufficiently small or the prescribed maximum iteration step number is covered.

4. Results and Discussions

(1) Experimental results

The bed contours at equilibrium condition in both cases are shown in **Fig.3**. It can be seen that the erosion around the upstream groin in Case 1 is deeper than that in Case 2. The maximum depths of scour hole around the upstream groin in Case 1 and 2 reach about 15cm and 2cm, respectively. The deposition area in Case 1 is concentrated in the downstream region of the downstream groin due to the reduction of the velocity and recirculation flows occurring in this region. On the other hand, in Case 2, the deposition area is distributed throughout the channel with a small concentration downstream of the downstream groin.

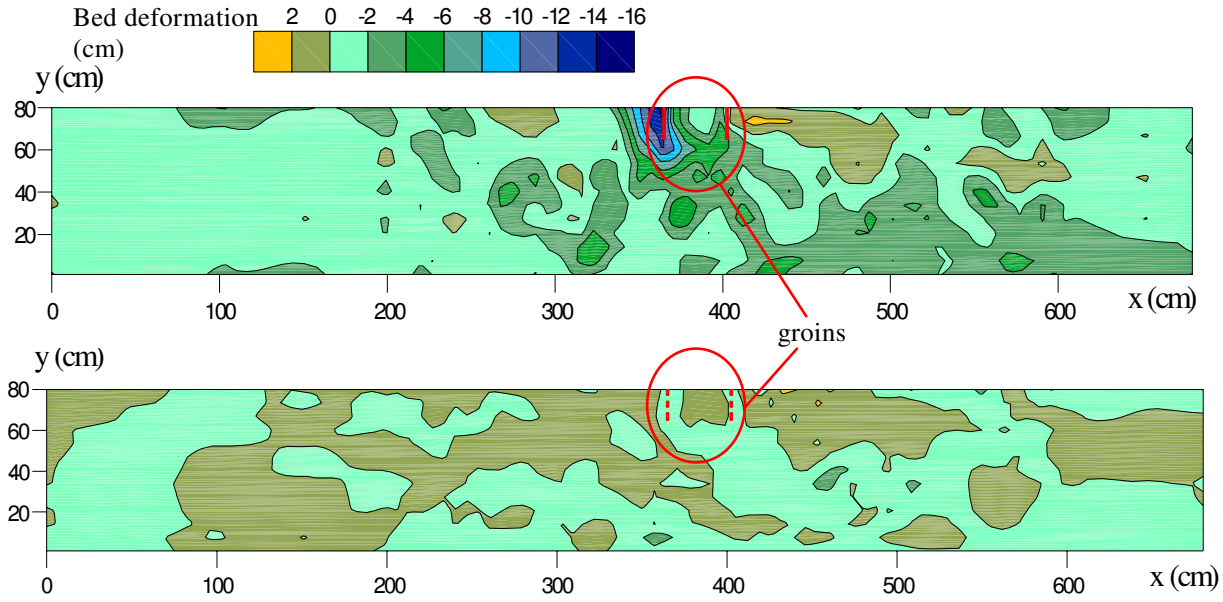

Fig. 3 Bed contours at equilibrium condition (top: Case 1 (impermeable groins); bottom: Case 2 (permeable groins))

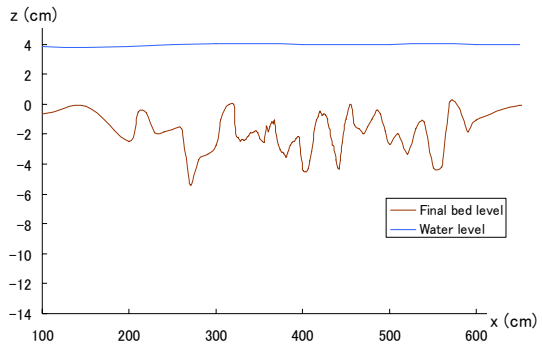

Fig. 4 Longitudinal profile of water surface and bed level along main channel (y=40cm) – Case 1.

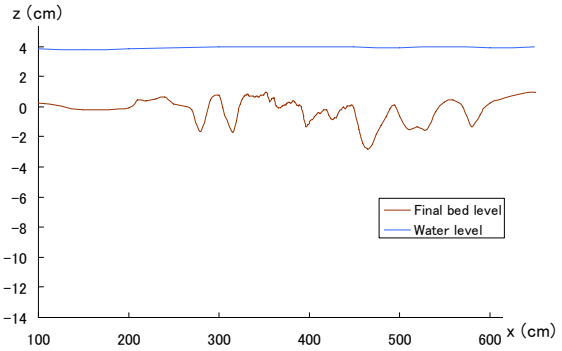

Fig. 5 Longitudinal profile of water surface and bed level along main channel (y=40cm) – Case 2.

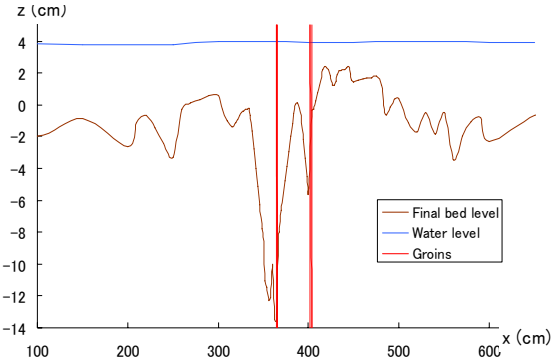

Fig. 6 Longitudinal profile of water surface and bed level along channel (y=72cm) – Case 1.

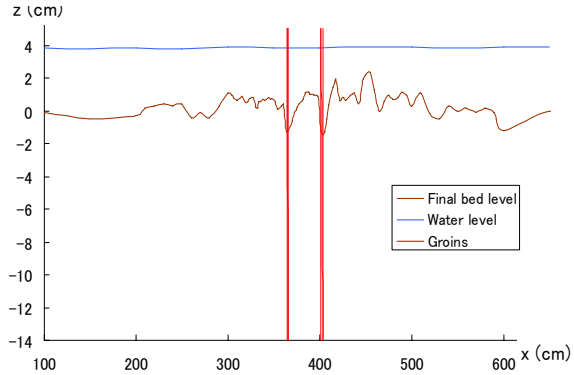

Fig. 7 Longitudinal profile of water surface and bed level along channel (y=72cm) – Case 2.

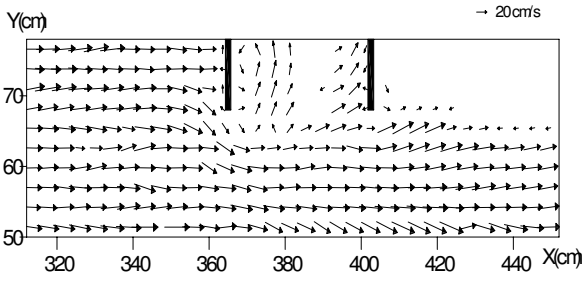

Fig.8 Velocity field around groins in XY plane at z=2.0cm – Case 1 (experiment).

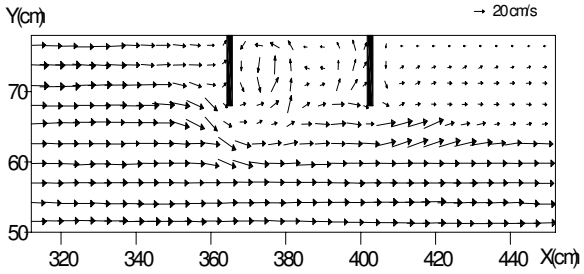

Fig.9 Velocity field around groins in XY plane at z=2.0cm – Case 1 (simulation).

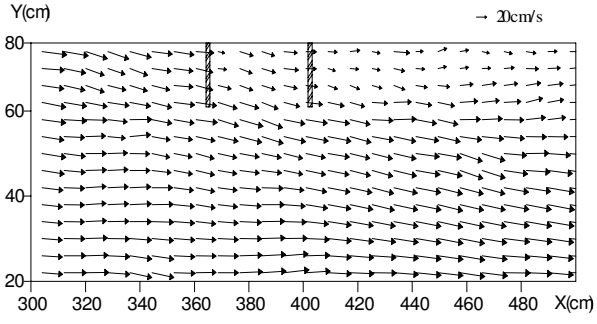

Fig.10 Velocity field around groins in XY plane at z=2.0cm – Case 2 (experiment).

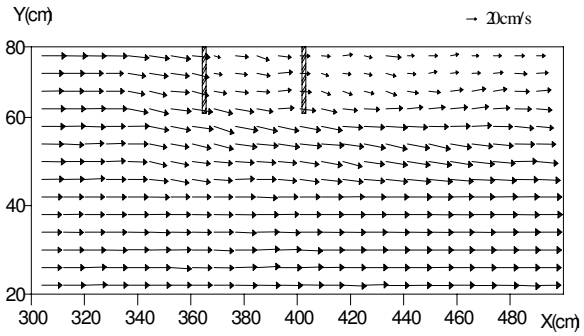

Fig.11 Velocity field around groins in XY plane at z=2.0cm – Case 2 (simulation).

The longitudinal profiles of water level and bed level along the channel (y=40cm and y=72cm) in Cases 1 and 2 are shown in **Fig.4**, **Fig.5**, **Fig.6** and **Fig.7**, respectively.

The level z=0cm denotes the initial bed level. The longitudinal section y=40cm corresponds to the centerline of the flume and y=72cm corresponds to the longitudinal section 8cm from the left wall of the channel. In both cases, a small increase of the water level near the groins can be seen, probably due to the effects of the contraction of the flow width by groins. The erosion deep around the groins in Case 1 can be seen with details in **Fig.5**.

(2) Comparison of numerical and experimental results

Numerical results of flow velocity are compared with those of measured ones based on the deformed fixed bed around groins of Case 1 and 2.

a) Velocity distribution around the impermeable groins in XY plane – Case 1 (z=2.0 cm)

The velocity distributions of experimental and simulated results around impermeable groins at depth z=2.0cm are shown in **Fig.8** and **Fig.9,** respectively. The magnitude of the simulated velocity agrees well with that of the experiment. When the flow approaches the upstream groin,

major part of the obstructed flow diverts to the main channel, which creates a mixing zone in front of the groin head. A part of the flow travels downstream which creates recirculation flow between the groins.

Comparing the simulation results with the experimental ones, the flow structures are quite similar in the upstream area of the groins but differ to some extent in the downstream area. A clear recirculation flow is observed in the simulation results comparing with the experimental results. One reason may be the measurement grid is too coarse for the experiment.

b) Velocity distribution around permeable groins in XY plane – Case 2 (z=2.0cm)

For the permeable groins, the velocity fields around the groins of experimental and simulated results are shown in **Fig.10** and **Fig.11**, respectively.

In this case, the flow directions are not greatly changed. It can be seen that just after passing the upstream groin, the flow direction diverts to the right side wall in the experimental results. At the downstream of the upstream groin, reduction of velocity occurs, but after the flow passed the downstream groin the reduction becomes more significant. The sediment deposition observed downstream of the downstream groin (see **Fig.3** bottom) could be caused by this velocity reduction.

Compared with Case 1 (impermeable groins), the flow patterns in Case 2 show practically parallel to the channel near the groins head.

c) Velocity distribution near the upstream groin in YZ plane – Case 1

The velocity vectors in YZ plane near the upstream groin of experimental and simulation results are shown in **Fig.12** and **Fig.13**, respectively.

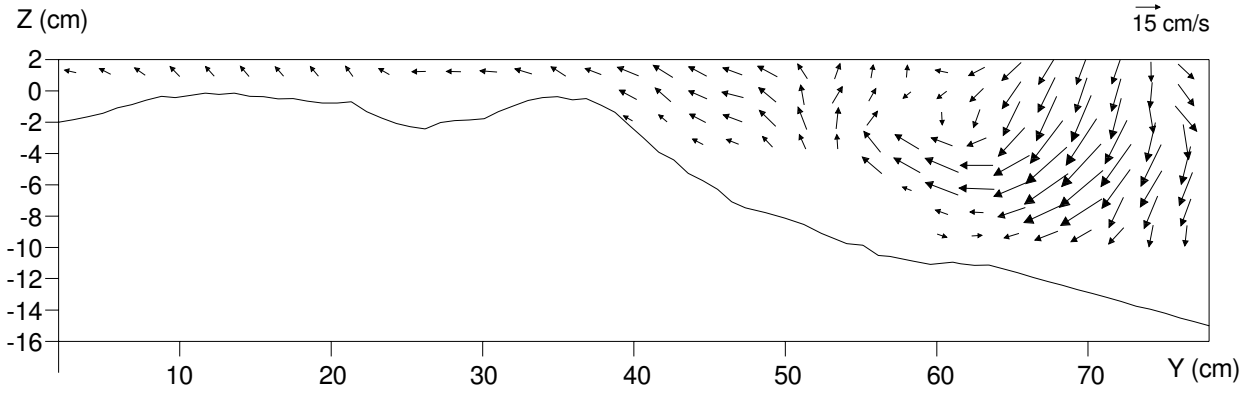

Fig.12 Velocity field around groins in YZ plane at x=362cm – Case 1 (experiment).

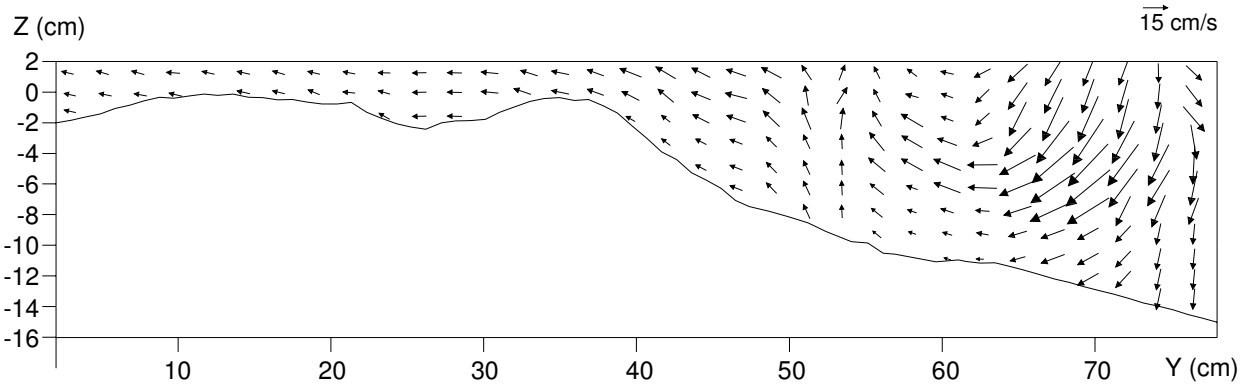

Fig.13 Velocity field around groins in YZ plane at x=362cm – Case 1 (simulation).

The longitudinal position of this cross section is x=362cm, just 2.25cm upstream of the upstream groin, seen from downstream to upstream.

From the experimental results, the recirculation flow near the upstream groin is quite similar to the computed results. The bed erosion around the upstream groin probably results from the influence of this recirculation flow that is more evident near the groin (from y=65cm to y=80cm). It means the flow is attacking the channel bank and can cause the erosion in this region. Hence bank protection measures are needed when this kind of groin is utilized.

The case of permeable groin is not shown here because the flow passing through the piles causes a little recirculation upstream of the upstream groin and without causing significant erosion compared with the case of impermeable groins (see **Fig.3** bottom).

5. Conclusions

The experiments have provided us with detailed information regarding the flow pattern and bed deformation around impermeable or permeable groins under non-submerged scour conditions.

Experimental result indicates the influence of the permeability on the bed deformation and flow structures around groins. Under the same hydraulic conditions, the erosion around the upstream groin is significantly deeper in the case of impermeable groins (Case 1) compared with the case of permeable groins (Case 2). The developed numerical model can simulate the flow structures around groins quite reasonably in fixed bed conditions, i.e., using final scoured bed form. Further 3D model simulations are expected in future works to validate the applicability of the numerical model in other cases such as movable bed and to compare the results with experimental data. The model should also be compared with field data where the results depend on the different conditions that are not considered in this study.

References

Ashida, K. and Michiue, M. (1972): Studies on bed load transportation for nonuniform sediment and river bed variation, Disaster Prevention Research Institute Annuals, Kyoto University, No. 14B, pp. 259-273 (in Japanese).

Carling, P.A., Kohmann, F., and Golz, E. (1996): River hydraulics, sediment transport and training works: their ecological relevance to European rivers, Archiv. Hydrobiol. Suppl., Vol. 113, No. 10, pp 129-146.

Garde, R. J., Subramanya, K. and Nambudripad, K. D. (1961): Study of scour around spur-dikes, Journal of Hydraulic Division, ASCE, Vol. 87, No. 6, pp. 23-38.

Gill, M.A. (1972): Erosion of sands beds around spur dikes, Journal of Hydraulic Division, ASCE, Vol. 98, No. 9, pp. 1587-1602.

Klaassen, G. J., Douben, K. and van der Waal, M. (2002): Novel approaches in river engineering, River flow 2002, Bousmar & Zech, eds., Swets & Zeitlinger, Lisse, pp. 27-42.

Kuhnle et al. (2002): Local scour associated with angled spur dikes, ASCE, Journal of Hydraulic Engineering, Vol. 128, No. 12.

Rodi, W. (1980): Turbulence models and their application in hydraulics- A state of art review, University of Karlsruhe, Germany.

Schwartz, R. and Kozerski, H. (2003): Entry and deposits of suspended particulate matter in groyne fields of the middle Elbe and its ecological relevance, Acta Hydrochim. Hydrobiol., Vol. 31, No. 4-5, pp 391-399.

Uijttewaal, W.S.J. (2005): Effects of groin layout on the flow in groin fields: laboratory experimental, Journal Hydraulic Engineering, ASCE, Vol. 131, No. 9, pp. 782-791.

Zhang, H. (2005): Study on Flow and Bed Evolution in Channels with Spur Dykes, Doctoral Dissertation, Kyoto University.

Zhang, H., Nakagawa, H., Muto, Y., Touchi, D. and Muramoto, Y. (2006a): 2D numerical model for river flow and bed evolution based on unstructured mesh, Journal of Applied Mechanics, JSCE, Vol. 9, pp. 783-794.

Zhang, H., Nakagawa, H., Muto, Y., Baba, Y. and Ishigaki, T. (2006b): Numerical simulation of flow and local scour around hydraulic structures, River flow 2006, pp. 1683-1693.

非越流条件での水制による流れと河床変動への影響

Hiroshi TERAGUCHI*・中川　一・武藤　裕則・馬場　康之・張　浩

*京都大学工学研究科

要　旨

この論文では，水制のまわりの流れと河床変動に関して実験および数値計算を行い得られた結果を示す。実験水路では一対の不透過または透過性の水制を左岸側に設置し，非越流の条件で水制周辺の流速を測定した。不透過水制の場合，水制周辺の上流での局所洗掘は透過水制の場合より深くなることが確認された。 非構造メッシュによる 3 次元数値モデルを開発し，数値計算を行った結果，流速は実験測定の結果を十分な精度で再現することができた。

キーワード：水制，非越流，3 次元数値モデル，非構造メッシュ